

Suppression of competing tunneling processes in thermally-activated carrier emission on self-assembled InAs quantum dots

A. Schramm,* S. Schulz, Ch. Heyn, and W. Hansen

Institute of Applied Physics, University of Hamburg, Hamburg, Germany

(Received 21 February 2008; revised manuscript received 1 April 2008; published 30 April 2008)

Electron emission from charged self-assembled InAs quantum dots is studied by means of deep level transient spectroscopy in strong magnetic fields applied parallel to the quantum-dot layer. Since a magnetic field oriented parallel to the quantum-dot layer strongly suppresses electron tunneling our experiments give valuable information about the contribution of tunneling processes to the emission. We probe both the low-temperature signal, which is found to be dominated by pure tunneling from the quantum-dot p states as well as the magnetic-field dependence of the thermally-activated emission. The thermally-activated emission from the s states is found to be only slightly affected by a parallel magnetic field. In contrast, for the thermally-activated emission from the p states, we find significant changes that we discuss in the frame of a thermally-activated tunneling model for the emission from multielectron states of the quantum dots. A conventional analysis of the decreasing tunneling rates in a parallel magnetic field yields an increase of apparent activation energies and capture cross sections of quantum dot p electrons. The results confirm that the tunneling path in thermally-activated processes becomes increasingly important with increasing occupation number of the dots.

DOI: [10.1103/PhysRevB.77.153308](https://doi.org/10.1103/PhysRevB.77.153308)

PACS number(s): 73.21.La

I. INTRODUCTION

Recently, much attention is paid to the emission of charge carriers from self-assembled InAs/GaAs quantum dots (QDs) embedded in pn or Schottky diodes.¹⁻⁷ Although the zero-dimensional quantum dot states are similar to electron traps in bulk material, they differ in both the confinement potential as well as the charge occupation, the latter being controlled by the diode voltage. In such a system, the emission process can be quite complex. It may comprise several emission paths consisting of, e.g., a thermal excitation to an excited state and a subsequent elastic tunneling process out of the dot. Competition of thermal and tunneling emission can occur depending on the samples under investigation and the applied electric field. This leads to several emission paths⁵ and combined emission processes, e.g., thermally-assisted tunneling.^{3,8} Thus, the analysis of time-resolved capacitance measurements [deep level transient spectroscopy (DLTS)] on self-assembled QDs is lively discussed and not completely understood.

With strong magnetic fields applied in DLTS experiments, we add further tessellate bricks in order to clarify the nature of the dominant emission processes. The use of magnetic fields in DLTS experiments is quite unconventional, but very helpful in order to study thermally-activated processes in QDs. Previously, we could show that magnetic fields applied perpendicular to the QD plane can be used to identify the QD p states having orbital momentums with $l \neq 0$.⁹ In the present Brief Report, we discuss experiments where strong magnetic fields are directed parallel to the QD plane (or perpendicular to the growth and emission direction). A parallel magnetic field strongly reduces the tunneling emission rate,¹⁰⁻¹³ while thermal emission should be essentially unaffected. Thus, with the magnetic field we can on the one hand identify the tunneling signal at low temperature, and on the other hand, we show how the magnetic field affects thermally-activated emission at elevated temperature. We present the behavior of the apparent activation energies and capture cross sections of

electrons emitted from the s and p shells as determined from a conventional Arrhenius analysis of the transients in parallel magnetic fields.

II. EXPERIMENTAL PROCEDURES

The sample was grown in a solid-source molecular beam epitaxy growth system on epi-ready, undoped GaAs (001) substrates. First, a highly Si-doped GaAs layer ($N_D = 3 \times 10^{18} \text{ cm}^{-3}$) was grown providing a back contact followed by a 1200 nm GaAs:Si ($N_D = 3.5 \times 10^{15} \text{ cm}^{-3}$) layer. The InAs dot layer is embedded in between 5 and 10 nm undoped GaAs layers. The QDs were grown at $T = 495 \text{ }^\circ\text{C}$ with a growth rate of $F = 0.01 \text{ ML/s}$ and coverage $\theta = 2.1 \text{ ML}$. Afterward, 750 nm slightly doped GaAs:Si ($N_D = 3.5 \times 10^{15} \text{ cm}^{-3}$) was grown. For atomic-force micrography, a second QD layer was deposited on the sample surface using the same growth parameters as for embedded QDs. Using standard optical lithography and lift-off techniques, Schottky contacts were formed by evaporation of 50 nm chromium for the top gate with a diameter of 1 mm. The back contact was provided by indium alloyed into the highly silicon-doped GaAs layer. The DLTS measurements were performed by using a Boonton capacitance meter in a helium bath cryostat with variable temperature.

III. RESULTS AND DISCUSSIONS

In Fig. 1, we show DLTS spectra obtained in the double-boxcar technique¹⁴ for different parallel magnetic fields. During a filling voltage pulse V_p with a duration $t_p = 1 \text{ ms}$, electrons are injected into the dots. These values ensure a complete filling of the QDs after t_p . The capacitance transient of the diode is recorded after the voltage has been reduced from the filling-pulse value to the reverse voltage V_{rev} . At V_{rev} , the dot layer is located within the depletion zone and the QD levels are lifted above the Fermi energy. The depth of

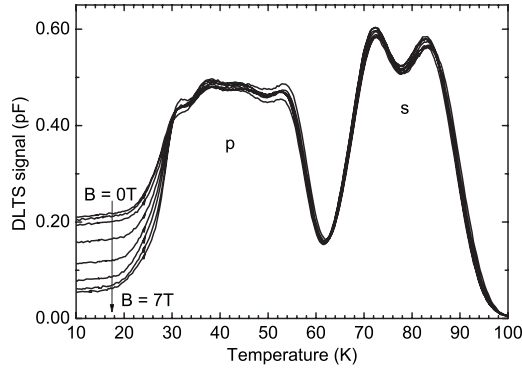


FIG. 1. DLTS spectra of a Schottky diode with embedded QDs. During the measurements, a magnetic field directed parallel to the QD layer is applied with values indicated in the figure. The field values were increased by steps of 1 T between adjacent traces. The reverse and pulse bias are $V_{rev} = -1.4$ V and $V_p = 0.7$ V, respectively. The rate window of the double-boxcar filter is $\tau_{ref} = 4$ ms with $t_2/t_1 = 8$.

the depletion zone depends on the QD occupation. The transients thus reflect the time evolution of the dot occupation. According to the boxcar-filter method, the DLTS signal depicted in Fig. 1 reflects the increase of the capacitance in the time interval $t_1 \leq t \leq t_2$. We observe pronounced DLTS maxima at $T = 80$ K and $T = 40$ K that we associate with the electron emission from the QD s and p states, respectively.³ The splitting of the s -state maximum is associated with different emission rates for quantum dots occupied with one and two electrons, respectively.^{3,9,15,16} Furthermore, a fine structure in the p maximum is discernible that we accordingly associate with emission from quantum dots occupied by one up to four electrons in the p state.⁹ Below $T < 20$ K, a temperature-independent background signal is observed which is generally associated with temperature-independent tunneling emission.^{4,6,17,18} In this temperature range, the signal strength in Fig. 1 strongly decreases in a parallel magnetic field providing further evidence that the signals indeed are caused by tunneling processes.¹⁰⁻¹³

In the following, we first discuss the magnetic field dependence of the low-temperature tunneling signal more quantitatively. Afterward, the much smaller effect of the magnetic field on the DLTS signal at higher temperatures is discussed. Assuming that at $T = 10$ K the DLTS signal results from pure tunneling processes, we determine a value for the barrier height within a simple semiclassical Wentzel-Kramers-Brillouin approximation (WKB) method. In our model, we assume at zero magnetic field a one-dimensional barrier potential $V(z) = E_{QD} - eFz - ne^2/(4\pi\epsilon\epsilon_0)[1/z_0 - 1/(z_0 + z)]$, where the last term considers the Coulomb field of the charge in the quantum dots.⁴ The barrier height with respect to the energy level from which tunneling starts is E_{QD} , the z coordinate points against growth direction, e is the electron charge, n is the number of electrons confined in the QD, ϵ the dielectric constant of GaAs, and F is the electric field induced by all charges in the Schottky diode except the charge within the QDs. The field induced by the QD charge is approximated by a Coulomb field of a metallic sphere of radius z_0 . For the calculation, we

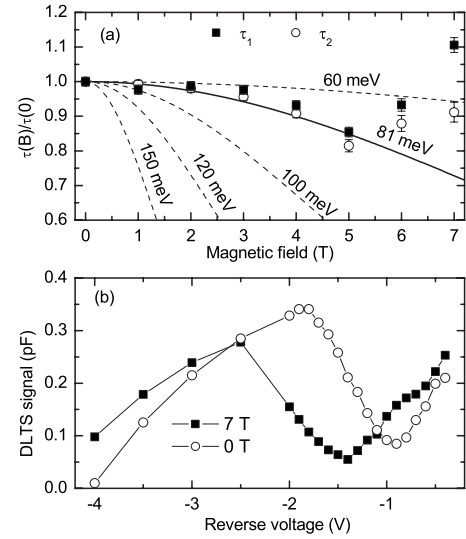


FIG. 2. (a) The dashed and full lines mark the calculated magnetic-field dependence of tunneling times normalized to zero-field tunneling times for various E_{QD} , $z_0 = 6$ nm and $n = 6$. The tunneling times τ_1 and τ_2 are obtained from an exponential approximation to the capacitance transients at $T = 10$ K using two time constants. The electric field is $F = 1.35 \times 10^6$ V/m as calculated for $V_{rev} = -1.4$ V at which the experimental data (squares) have been recorded. (b) shows DLTS signals at $T = 10$ K and $\tau_{ref} = 4$ ms with (full squares) and without (open circles) applied magnetic field. The lines connecting the data points are guides to the eye only.

assume a dot occupation with $n = 6$ electrons, i.e., completely filled s and p shells. We consider the effect of the parallel magnetic field by adding to $V(z)$ the term $\frac{e^2 B^2}{2m^*}(z - z_1)^2$, where z_1 is the distance between the depletion zone boundary and the dot layer and m^* is the effective mass in GaAs. The tunneling emission rate τ^{-1} in our semiclassical WKB approach is proportional to¹²

$$\tau^{-1}(B) \sim \exp\left(-\frac{\sqrt{8m^*}}{\hbar} \int_0^{z_1} \sqrt{V_B(z)} dz\right), \quad (1)$$

with $V_B(z) = V(z) + \frac{e^2 B^2}{2m^*}(z - z_1)^2$. Calculated ratios $\tau(B)/\tau(0)$ are displayed for different barrier heights in Fig. 2(a) together with experimental values obtained from an exponential approximation to the measured capacitance transients at $T = 10$ K and $V_{rev} = 1.4$ V. Generally, the obtained capacitance transients determined from the QD carrier relaxation are nonexponential due to multioccupancy of QD levels and inhomogeneous broadening of the QD ensemble. Therefore, we have to apply exponential fits with more than one time constant.¹⁴ An exponential approximation with two time constants τ_1 and τ_2 already gives satisfying results. At $B = 0$ T, we obtain $\tau_1 = 4.1$ ms and $\tau_2 = 50.9$ ms. In Fig. 2(a), the time constants that best describe the transient in magnetic field are depicted. The behavior of the time constants up to $B = 5$ T is well described with the calculation assuming a barrier height $E_{QD} = 81$ meV. It will turn out that this value is in close correspondence with the barrier height expected from the thermal emission data at higher temperature discussed later (see Fig. 4). The time constants extracted at B

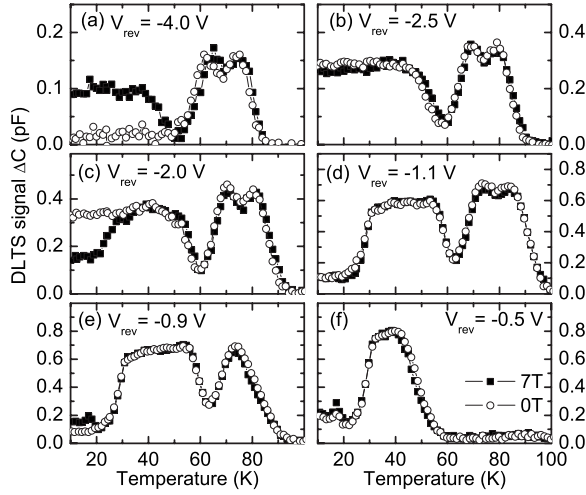


FIG. 3. DLTS spectra at $B=7$ T (full squares) and $B=0$ T (open circles) directed parallel to the QD layer. The reverse voltages V_{rev} are (a) -4.0 V, (b) -2.5 V, (c) -2.0 V, (d) -1.1 V, (e) -0.9 V, and (f) -0.5 V and the pulse bias is $V_p=0.7$ V. The rate window of the double-boxcar filter is $\tau_{ref}=4$ ms with $t_2/t_1=8$.

≥ 6 T deviate from the calculated ratios. We believe that for these magnetic fields another emission process starts to dominate. In high magnetic fields tunneling processes from wetting layer (WL) states become apparent and their time constants fit into the used rate window. This assumption is substantiated in Fig. 1, in which the decrease of the tunneling background is starting to level off for $B \geq 6$ T at 0.05 pF. Our results confirm that the low-temperature DLTS signal in Fig. 1 is mainly caused by pure tunneling processes from the QD p shell.

The tunneling process strongly depends on the electric field which we vary by the reverse bias V_{rev} . The behavior of the DLTS signal with V_{rev} is depicted in Fig. 2(b). The open circles and filled squares denote the DLTS signals measured at $B=0$ and 7 T, respectively. For the used rate window of $\tau_{ref}=4$ ms, the $B=0$ T data reveal a maximum at $V_{rev}=-1.8$ V. The behavior of the signal can be understood considering the signal of the boxcar filter if the tunneling rate is tuned with the electric field. At the maximum, the tunneling time matches $\tau_{ref}=4$ ms. Smaller signals arise when the tunneling time deviates to larger and smaller values at lower and higher fields, respectively. A parallel magnetic field obviously shifts the maximum to a lower $V_{rev}=-2.5$ V. This can be qualitatively explained by the reduction of tunneling rates in the magnetic field: A higher electric field (lower V_{rev}) has to be applied in order to recover the same tunneling rate.

In Fig. 3, we present typical DLTS spectra recorded at different reverse voltages for $B=0$ and 7 T. The data demonstrate that at all reverse voltages, the spectra only appreciably change with the magnetic field in the tunneling regime at low temperature. Furthermore, the behavior of the signal arising from low-temperature tunneling strongly depends on the choice of V_{rev} . Note that it only decreases in a certain range of V_{rev} . At $V_{rev}=-4.0$ V in Fig. 3(a), the temperature-independent DLTS signal below $T \approx 50$ K is increased for $B=7$ T in contrast to the tunneling background in Fig. 1. Obviously, no influence of B on the DLTS spectra is ob-

served at $V_{rev}=-2.5$ V [Fig. 3(b)], whereas the tunneling background is suppressed at $B=7$ T in Fig. 3(c), similar to Fig. 1. Again, for $V_{rev}=-1.1$ V in Fig. 3(d), the amplitudes of DLTS signals arising from tunneling processes are similar. Further increase of V_{rev} leads again to a higher tunneling background for $B=7$ T and additionally to the disappearance of high-temperature DLTS signals. The latter arises since part of the QD levels remain below the Fermi energy at the reverse voltage. At $V_r=-0.5$ V, the DLTS signals arising from tunneling seem to be similar again. The behavior can be easily understood by means of Fig. 2(b). At the interception points of the $B=0$ and 7 T data, we expect the behavior of the DLTS signal arising from the tunneling background in Fig. 3 to reverse its magnetic field behavior. Furthermore, we point at a DLTS peak at $T \approx 17$ K that arises below $V_{rev} < -1.0$ V. We associate this peak with the thermal emission from WL states. The peak appears at high reverse voltages, $V_{rev} > -1.0$ V, where tunneling is suppressed. Also, once discernible, the peak is more pronounced in high magnetic fields. These observations are in accordance with the assumption that an additional tunneling process is observed at $B \geq 6$ T when we quantitatively determine time constants from the low-temperature transients that cause the tunneling signals in Fig. 1.

Finally, we evaluate the DLTS maxima observed at $T > 20$ K in Fig. 1. Obviously, the signal only slightly changes with the magnetic field confirming that the signal at these temperatures mainly arise from thermal activation processes. In previous publications, emission paths have been suggested that consist of a thermal activation to a bound state in the QD, e.g., the p state, and a subsequent tunneling process.^{6,7,18} For an emission path consisting of thermal excitation from the s to the p state and a subsequent tunneling, we would expect a drastic reduction of the signal in parallel magnetic field accompanied with a significant change of the maximum position. In contrast, only slight changes are observed in our data so that we exclude this emission path for the signal associated with the emission from the QD s state. The slight changes that are discernible in the spectra we associate to thermally-assisted tunneling (TAT),^{3,8} involving QD states that arise from the tunnel interaction with the continuum close to the band edge of the barrier material. From the TAT model, we expect that due to tunneling close to the top of the barrier the effective binding energy will be slightly reduced with respect to the value expected from a purely thermal emission.

In a first approach, we apply a conventional Arrhenius analysis of the maxima positions in the spectra recorded at different reference times. In the double-boxcar method assuming an exponential decay according to $C(t)=C_\infty - \Delta C_0 \exp(-e_n t)$, the emission rate at the maxima in the DLTS spectrum is given by $e_n = \tau_{ref}^{-1}$, where $\tau_{ref} = (t_2 - t_1) / \ln(t_2/t_1)$ is the reference time.¹⁴ C_∞ and ΔC_0 are the steady state capacitance and the change of the capacitance due to the emission, respectively. The activation energy E_a and electron capture cross section σ_a are determined from the temperature dependence of the emission rate $e_n(T) = \sigma_a \gamma T^2 \exp(-E_a/kT)$, where γ is a temperature-independent constant and k the Boltzmann constant. The thus determined apparent activation energies E_a and electron capture cross

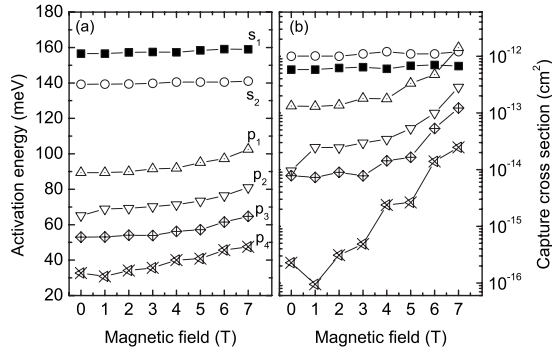


FIG. 4. (a) Activation energies E_a and (b) capture cross sections σ_a of QD levels for various parallel magnetic fields at $V_{rev} = -1.4$ V.

sections σ_a for the s and p maxima are depicted in Fig. 4. We observe that E_a and σ_a slightly increase with the magnetic field. The increase of E_a for s -electron emission amounts to only 2 meV. This value is smaller than the difference between the s -level activation energy and the barrier height E_{QD} that we derive from the TAT model, which is of the order of 10 meV at zero magnetic field.¹⁹ According to the TAT model the deviation of the zero-field p -state barrier height from the apparent activation energy is much stronger for the p state. We find⁴ that the contribution of the Coulomb field to the tunneling barrier in charged dots significantly increases the tunneling rates. Thus, the apparent activation energy decreases with the dot occupation. Again, we explain the observed increase of E_a in the parallel magnetic field with a suppression of tunneling paths in the thermally-assisted tunneling processes. The stronger impact of B on the p states compared to the s states can be explained with the higher charge state and with the lower emission temperature. Furthermore, from the analysis of the tunneling data, it is apparent that at the fields used in these experiments the di-

rect tunneling from p states is significant. It competes with the thermally-activated emission hampering the thermal analysis of the data corresponding to emission from the $n = 6$ state. We expect the apparent activation energies E_a to approach the respective barrier heights at high magnetic fields.

IV. CONCLUSION

To conclude, we discuss thermally-activated as well as tunneling emission processes in DLTS experiments on self-assembled InAs QDs in strong magnetic fields oriented parallel to the QD layer. A parallel magnetic field leads to a decrease of tunneling rates in competing tunneling paths in the thermally-activated emission process that is established in an increase of apparent activation energies and capture cross sections of QD states with higher magnetic fields. Thus, the importance of combined emission paths can be evaluated with these experiments. Our data confirm a thermally-assisted tunneling model. Within this model the s -state emission is only slightly affected by tunneling processes close to the top of the barrier. No signature of a process is found that involves thermal excitation from the s to the p state and subsequent tunneling. Furthermore, as expected from the model, the increase in the apparent activation energies is stronger for emission from the p state. By modeling the tunneling times in magnetic fields, we give strong evidence that temperature-independent low-temperature DLTS signals stem from pure tunneling emission from p states.

ACKNOWLEDGMENT

The authors acknowledge the Deutsche Forschungsgemeinschaft (DFG) for financial support via SFB 508 “Quantum materials.”

*Present address: Optoelectronics Research Centre, Tampere University of Technology, Finland. andreas.schramm@tut.fi

¹M. Geller, E. Stock, C. Kapteyn, R. L. Sellin, and D. Bimberg, Phys. Rev. B **73**, 205331 (2006).

²M. Geller, A. Marent, E. Stock, D. Bimberg, V. I. Zubkov, I. S. Shulgunova, and A. V. Solomonov, Appl. Phys. Lett. **89**, 232105 (2006).

³S. Schulz, S. Schnüll, C. Heyn, and W. Hansen, Phys. Rev. B **69**, 195317 (2004).

⁴S. Schulz, A. Schramm, C. Heyn, and W. Hansen, Phys. Rev. B **74**, 033311 (2006).

⁵O. Engström and P. T. Landsberg, Phys. Rev. B **72**, 075360 (2005).

⁶O. Engström, M. Kaniewska, W. Jung, and M. Kaczmarczyk, Appl. Phys. Lett. **91**, 033110 (2007).

⁷O. Engström, M. Kaniewska, M. Kaczmarczyk, and W. Jung, Appl. Phys. Lett. **91**, 133117 (2007).

⁸G. Vincent, A. Chantre, and D. Bois, J. Appl. Phys. **50**, 5484 (1979).

⁹A. Schramm, S. Schulz, J. Schaefer, T. Zander, C. Heyn, and W. Hansen, Appl. Phys. Lett. **88**, 213107 (2006).

¹⁰I. E. Itskevich, T. Ihn, A. Thornton, M. Henini, T. J. Foster, P. Moriarty, A. Nogaret, P. H. Beton, L. Eaves, and P. C. Main, Phys. Rev. B **54**, 16401 (1996).

¹¹R. J. Luyken, A. Lorke, A. O. Govorov, J. P. Kotthaus, G. Medeiros-Ribeiro, and P. M. Petroff, Appl. Phys. Lett. **74**, 2486 (1999).

¹²A. Patane *et al.*, Phys. Rev. B **65**, 165308 (2002).

¹³B. Ivlev, Phys. Rev. A **73**, 052106 (2006).

¹⁴D. V. Lang, J. Appl. Phys. **45**, 3023 (1974).

¹⁵O. Engström, M. Malmkvist, Y. Fu, H. O. Olafson, and E. O. Sveinbjörnsson, Appl. Phys. Lett. **83**, 3578 (2003).

¹⁶A. Schramm, J. Schaefer, S. Schulz, C. Heyn, and W. Hansen, AIP Conf. Proc. **893**, 833 (2007).

¹⁷M. Baj, P. Dreszer, and A. Babinski, Phys. Rev. B **43**, 2070 (1991).

¹⁸C. M. A. Kapteyn, F. Heinrichsdorff, O. Stier, R. Heitz, M. Grundmann, N. D. Zakharov, P. Werner, and D. Bimberg, Phys. Rev. B **60**, 14265 (1999).

¹⁹S. Schulz, A. Schramm, T. Zander, C. Heyn, and W. Hansen, AIP Conf. Proc. **772**, 807 (2005).